Calibration of two-dimensional floodplain modeling in the Atchafalaya River Basin using SAR interferometry

Hahn Chul Jung,[1]* Michael Jasinski,[1] Jin-Woo Kim,[2] C. K. Shum,[2] Paul Bates,[3] Jeffrey Neal,[3] Hyongki Lee,[4] and Doug Alsdorf[2]

[1]Hydrological Sciences Laboratory, NASA Goddard Space Flight Center, Greenbelt, MD 20871, USA

[2]Division of Geodetic Science, School of Earth Sciences, Ohio State University, Columbus, OH 43210, USA

[3]School of Geographical Sciences, University of Bristol, University Road, Bristol BS8 1SS, UK

[4]Department of Civil and Environmental Engineering, University of Houston, Houston, TX 77004, USA

*Corresponding Author

Hahn Chul Jung

Hydrological Sciences Laboratory, Code: 617

NASA Goddard Space Flight Center

Building 33, Greenbelt Road, Greenbelt, MD 20771, USA

Email: hahnchul.jung@nasa.gov

Phone: 301-614-6839

Submitted to Water Resources Research

Abstract

Two-dimensional (2D) satellite imagery has been increasingly employed to improve prediction of floodplain inundation models. However, most focus has been on validation of inundation extent, with little attention on the 2D spatial variations of water elevation and slope. The availability of high resolution Interferometric Synthetic Aperture Radar (InSAR) imagery offers unprecedented opportunity for quantitative validation of surface water heights and slopes derived from 2D hydrodynamic models. In this study, the LISFLOOD-ACC hydrodynamic model is applied to the central Atchafalaya River Basin, Louisiana, during high flows typical of spring floods in the Mississippi Delta region, for the purpose of demonstrating the utility of InSAR in coupled 1D/2D model calibration. Two calibration schemes focusing on Manning's roughness are compared. First, the model is calibrated in terms of water elevations at a single *in situ* gage during a 62 day simulation period from 1 April 2008 to 1 June 2008. Second, the model is calibrated in terms of water elevation changes calculated from ALOS PALSAR interferometry during 46 days of the image acquisition interval from 16 April 2008 to 1 June 2009. The best-fit models show that the mean absolute errors are 3.8 cm for a single *in situ* gage calibration and 5.7 cm/46 days for InSAR water level calibration. The optimum values of Manning's roughness coefficients are 0.024/0.10 for the channel/floodplain, respectively, using a single *in situ* gage, and 0.028/0.10 for channel/floodplain the using SAR. Based on the calibrated water elevation changes, daily storage changes within the size of ~230 km^2 of the model area are also calculated to be of the order of 10^7 m^3/day during high water of the modeled period. This study demonstrates the feasibility of SAR interferometry to

support 2D hydrodynamic model calibration and as a tool for improved understanding of complex floodplain hydrodynamics.

1. Introduction

The Atchafalaya River Basin, a low-lying catchment in southern Louisiana consisting of wetlands and bayous, is the principal distributary of the Mississippi River. Given both its proximity and make-up, the Atchafalaya basin plays an important role in mitigating floods and preserving wetland resources in coastal Louisiana. For example, Mississippi River floodwaters in May 2011, resulting from unusually high precipitation in the watershed, were diverted through the Morganza Spillway into the Atchafalaya River Basin to prevent major inundations in populated cities including Baton Rouge and New Orleans [USACE, 2011]. Also, flood damage caused by Hurricane Katrina in August 2005 and Hurricane Rita in September 2005, although significant, was mitigated by flooding into the Atchafalaya basin [LPBF, 2008; Knabb *et al*, 2006, 2007]. Flood management has been enabled through the construction of levees, bank protection and spillways along the Lower Mississippi River, the Atchafalaya, and their tributaries.

Although the man-made levees and river diversions abate flood damage, they also disrupt the natural floodplain environment. Of principal concern is the reduction by more than 50% in the historically large sediment loads deposited within the Lower Mississippi River delta [LPBF, 2010], which is a major factor in the land loss in southeastern Louisiana [Meade, 1995]. Annual wetland loss in Louisiana has been estimated at 100–150 km^2 and the loss rate is increasing exponentially [Walker *et al*., 1987; Templet and Meyer-Arendt, 1988], although the Atchafalaya wetland is actually increasing in size. Comprehensive flood control and wetland loss studies on coastal Louisiana including the Atchafalaya River Basin have been initiated to further the understanding of its important role [USEPA, 1987].

Despite its importance to the Atchafalaya basin, knowledge of its floodplain dynamics remains poor. This is primarily due to a lack of *in situ* gage measurements in the floodplain. Most operational gages are located along main river channels and bayous for practical and economic reasons and rarely in floodplains [Allen *et al*., 2008; Kim *et al*., 2009]. Thus, despite long historical data records for the channels, there are insufficient *in situ* data for detailed calibration of 2D models resulting in limited accuracy [Allen *et al*., 2008]. This is because water flow across wetlands is more complex than channel routing [Alsdorf *el al*., 2007; Jung *et al*., 2010] as flow paths and water sources are not constant in space and time, but rather vary with floodwater elevations. Therefore, 2D flood modeling combined with emerging remotely sensed data would greatly facilitate the investigation of the temporal and spatial variations of the floodplain water movement and further the understanding of the linkage between channels and floodplains.

The first popular approach to fluvial hydraulics modeling was one-dimensional finite difference solutions of the full St. Venant equations along the river reach [e.g. Fread, 1984; Samuels, 1990; Ervine and MacLeod, 1999] since the 1D model design and implementation are simple and computationally efficient (e.g. MIKE11 [DHI Water and Environment, 2001], ISIS [Halcrow and HR Wallingford, 2001], FLUCOMP [Samuels and Gray, 1982] and HEC-RAS [USACE, 2001]). However, when applied to floodplain flows, the 1D model cannot simulate lateral diffusion of the flood wave. This is because floodplain topography is discretized as cross-sections rather than as a surface and flow depends on the location and orientation of finite cross-section measurements [Hunter *et al*., 2008].

The advances in computing resources and the growing availability of spaceborne data have enhanced the opportunities to estimate flood inundation extent, floodplain water elevation, and to model floodplain hydrodynamics [Hess *et al*, 1995; Smith, 1997; Alsdorf *et al*., 2000; Bates *et al*., 1992]. For instance, high-resolution Light Detection And Ranging (LiDAR) elevation maps enable modelers to represent an improved spatial resolution of channel and floodplain hydraulics that are consistent with known processes [Bates *et al*., 2005]. Repeat-pass synthetic aperture radar (SAR) interferometry has recently been employed to estimate water level changes with time [Alsdorf *et al*. 2000] and when combined with modeling storage changes [Alsdorf, 2003] and flow hydraulics [Alsdorf *et al*., 2005]. Satellite SAR interferometry offers the opportunity to characterize complex fluvial environments in combination with sparse *in situ* gages and satellite altimetry [Kim *et al*., 2009; Lu *et al*., 2009; Lee *et al*., 2009; Jung *et al*., 2010]. The floodplain waters and lake habitats can provide double-bounce backscattering, which allows SAR interferometric coherence to be maintained and provides water elevation changes [Lu *et al*., 2005; Lu and Kwoun, 2008; Jung and Alsdorf, 2010].

Two-dimensional models in conjunction with suitably resolved and accurate digital elevation models (DEMs) of the channel and floodplain surface, and with suitable inflow and outflow boundary conditions, allow the water depth and depth-averaged velocity to be computed [Bates *et al*., 2005]. Many 2D hydraulic modeling approaches discretized the floodplain as a high resolution regular grid [e.g. TUFLOW [Syme, 1991], DIVAST [Falconer, 1986], TRENT [Villanueva and Wright, 2006], JFLOW [Bradbrook *et al*., 2004], and LISFLOOD-FP [Bates and De Roo, 2000], and structured grid 2D flood inundation modeling has been widely used to predict floodplain inundation since first proposed by Zanobetti *et al*. (1970).

The work presented here complements previous investigations of Atchafalaya River hydrology. For example, previous modeling studies have focused on the spatial and volumetric changes of water, sediment, and salinity in the delta and coastal regions located at outlets of the Atchafalaya River Basin [e.g. Donnell *et al*., 1991; Donnell and Letter, 1992; Wang *et al*., 1995; Vaughn *et al*., 1996]. However, these studies did not implement 2D hydrodynamic modeling to reveal the floodplain water variations within the levee-protected areas. Other studies using SAR interferometry showed the feasibility to measure floodplain water elevation changes in combination with *in situ* measurements and altimetry [Lu *et al*., 2005; Lu and Kwoun, 2008; Lee *et al*., 2009; Kim *et al*., 2009]. These studies were focused on the number of SAR data acquisition and areas of coverage. Other studies using visible and infrared Landsat imagery have delineated land-water classification within the Atchafalaya River Basin [Allen *et al*., 2008].

2. Study Objective

The calibration of 2D floodplain modeling investigations is usually limited by few or no water level gages in the floodplain. In many counties, post-flood field surveys are conducted to determine flood damage and extent. While coupled 1D/2D flood modeling offers improved estimation of inundation extent, few studies are able to validate detailed spatial variations in floodplain water elevations. Remote sensing methods for flood inundation extent were utilized to measure the fitness of the floodplain model results [e.g. Wilson *et al*., 2005; Di Baldassarre *et al*., 2009]. Few modeling studies have taken advantage of current satellite SAR interferometric phase measurements of water elevation changes since the SAR interferometric processing is not straightforward to generate the hydrologic products for the specified model use.

The goal of the present study is to investigate to what extent SAR interferometry can be used to improve model calibration. Specifically, the 2D LISFLOOD-ACC model [Bates *et al*., 2010] is applied to the central Atchafalaya River Basin together with repeat-pass interferometry from the Advanced Land Observing Satellite (ALOS) Phased Array type L-band Synthetic Aperture Radar (PALSAR). LISFLOOD provides 1D diffusive channel flow and 2D simplified shallow water floodplain flow [Bates *et al*., 2010]. Satellite InSAR data, namely PALSAR, are used to derive flood levels changes and water surface slopes at times of SAR data acquisitions.

LISFLOOD is calibrated using two different approaches, both focusing primarily on Manning's equation. First, a traditional approach using gage measurements is employed. Second, the same model is calibrated using the 2D water level and slope data extracted from two PALSAR interferometric images, acquired 46 days apart. The results of both approaches are compared and the merits and disadvantages of each are discussed. The PALSAR-derived floodplain water elevation change is also used to generate time series of water storage change in the model area.

This study offers to add new insights in 2D hydrodynamic modeling particularly in floodplain environments. The complexity of floodwaters has not been well captured because floodwaters move laterally across wetlands and this movement is not bounded like that of typical channel flow. This study of 2D hydrodynamic modeling and implementation of SAR interferometry for model calibration aims to improve our understanding of the Atchafalaya floodplain dynamic knowledge and provide an opportunity to investigate the impacts of flood hazard in the coastal Louisiana regions.

3. Study Area

The Atchafalaya River Basin is located west of the Lower Mississippi River in south Louisiana within the coastal margin of the Gulf of Mexico. This region includes about 2,500 km^2 of the Nation's most significant extents of bottomland hardwoods, swamps, bayous, and backwater lakes [Allen *et al*., 2008]. The Atchafalaya River's immense floodplain is bounded on the east and west sides by levees. Gates along the main stem are used to divert nearly 30% of the Mississippi River water into the Atchafalaya and this flows south through the floodplain to the Gulf of Mexico along approximately 225 km of river reach [LDNR, 2010; Kim *et al*., 2009].

As a consequence of frequent flooding, the basin is a sparsely populated area holding a rich abundance and diversity of terrestrial and aquatic species. In the spring, the basin receives well-oxygenated water carrying high loads of sediment and nutrients [Allen *et al*., 2008]. In addition to the Atchafalaya River, Wax Lake Outlet inside the Six Mile Lake Water Management Unit (WMU) governs the outflow from the levee protected basin to the Gulf of Mexico for water management.

Figure 1 shows the location map including rivers, levees, gages, ALOS PALSAR swath, and model area. The USGS National Wetlands Research Center and the U.S. Army Corps of Engineers (USACE) provide current stage data on nearly three dozen stations in the basin. Gage stations used in this study are indicated in Figure 1.

The USACE has identified 13 subbasins or WMUs because of morphological diversity within the basin [USACE, 1982]. Figure 2 shows the WMUs outlined in gray. Because of the unique character of each WMU, fluctuating river levels can result in very different patterns of water distribution among the WMUs. The seasonal flow of water through the basin is critical to maintaining its ecological integrity.

For the current study, LISFLOOD is applied specifically to the Buffalo Cove WMU, an area of 230 km^2 in the central Atchafalaya River Basin (See Figure 1, 2). The WMU is characterized by a swamp forest with paths of slowly moving water or bayous. This WMU is selected because of the proximity of *in situ* and satellite measurements, and because its upstream, downstream, and lateral boundaries are well defined. Buffalo Cove is surrounded by the main channel on the east and a levee on the west (Figure 2) with water level gage stations at Myette Points (C3) in the channel and Buffalo Cove (B1) in the bayou, shown in Figure 3. Moreover, the Buffalo Cove and Upper Bell River WMUs show clearer flow pattern of floodwater in the PALSA interferometric phase as compared to any other WMUs (Figure 4). This provides more spatial variation in water elevation changes and is therefore a more rigorous test of the floodplain model performance.

4. Methods and Data

4.1. Hydrodynamic Model

An inertial and parallel version of LISFLOOD-FP hydrodynamic model, or LISFLOOD-ACC [Bates and De Roo, 2000; Bates *et al*., 2010], is applied to the Buffalo Cove WMU. LISFLOOD-ACC is a simplified shallow water model that allows the use of a larger stable time step than previous LISFLOOD-FP variants, and hence quicker run times in addition to a better representation of the flow physics [Bates *et al*., 2010; Neal *et al*., 2011]. Channel flow is represented using the diffusive approximation to the full 1D St. Venant equations solved using a fully implicit Newton-Raphson scheme. Floodplain flows decoupled in x and y are implemented for a raster grid to give an approximation to a 2D inertial wave. Mass conservation was simulated through the continuity equation (Equation 1). The LISFLOOD-ACC momentum equation includes the gravity and local acceleration terms from the shallow water equations but not the convective acceleration and is solved using an explicit finite difference scheme (Equation 2).

$$h_{i,j}^{t+\Delta t} = h_{i,j}^{t} + \Delta t \frac{Q_{xi,j-1}^{t} - Q_{xi,j}^{t} + Q_{yi,j-1}^{t} - Q_{yi,j}^{t}}{\Delta x^2} \tag{1}$$

$$Q^t = \frac{q^t - g\hbar_{flow}^{t}\Delta t \frac{\Delta\left(\hbar^t + z\right)}{\Delta x}}{\left(1 + g\hbar_{flow}^{t}\Delta t n^2 \left|q^{t-\Delta t}\right| / \left(\hbar_{flow}^{t}\right)^{10/3}\right)} \Delta x \tag{2}$$

where h is the cell water depth, h_{flow} is the depth between cells through which water can flow, Q is the flow between cells, Δx is the cell size, n is Manning's roughness coefficient, q is Q from the previous time step divided by cell width and g is gravity. Model implementation involves use of the diffusive solver for channel flow and Equations (1) and (2) for 2-D inundation flow modeling, which has been parallelized using the shared memory Open Multi Processor (OpenMP) [Neal *et al*., 2009] to reduce model run time.

The Buffalo Cove model was run over a 62-day simulation period from 1 April 2008 to 1 June 2008 to accommodate at least two ALOS PALSAR acquisition dates on April 16 2008 and 1 June 2008. Figures 3a and 3b illustrate that the simulation period runs during high flow conditions associated with upper Mississippi River basin snowmelt and spring rains, typical for this time of year.

Inputs include floodplain topography, bathymetric depths, channel widths, flow boundary conditions, and Manning's roughness coefficients for channels (n_C) and floodplains (n_F). The floodplain topography was constructed using a high resolution 1 m LiDAR DEM of the whole basin published by USGS National Geospatial Program and USGS Coastal and Marine Geology Program [USGS, 2011]. The LiDAR survey was acquired in November 2010 during an optimal data collection window in terms of average river stage, average minimum temperature, and tree canopy as compared to the previous LiDAR data collections in years of 2000, 2002, and 2003. The vertical accuracy requirements meet or exceed the required RMSE of 18.5 cm. The 1 m LiDAR data was aggregated to 90 m to decrease grid resolutions and reduce model run time. The pixel-to-pixel noise is uncorrelated and reduces linearly in proportion to $1/\sqrt{n}$ as the data are aggregated, where *n* is the number of pixels being averaged [Rodriguez *et al*., 2006]. The input LiDAR noise for model grids at 90 m is less than 0.2 cm. The averaging can result in a terrain data error due to smoothing out hydraulically relevant topography. This resolution has been shown in a number of previous studies to be appropriate to predict flood inundation in rural areas providing care is taken over the representation of linear features, such as embankments or levees, which can control the flow development [Bates and De Roo, 2000; Horritt and Bates, 2001]. Levees in the domain are narrow, typically less than 10 m wide and are sufficiently high so that floodwaters cannot overtop them for the chosen simulation period. In order to handle these subgrid-scale features [Yu and Lane, 2011], the levees in 1 m resolution are vectorized, extracted, and input into the 90 m resolution floodplain topography directly, without averaging out adjacent elevations that would have resulted in an uncharacteristically low height at 90 m resolution.

Bathymetry was based on USACE data. The USACE developed updated flood control, navigation maps, and hydrographic survey maps for the Atchafalaya River as part of a comprehensive mapping project [USACE, 2006]. The mapping project provided bathymetric depth measurements every ten feet along the river cross sections. Based on the bathymetry dataset, the average bed elevations and channel widths were calculated as equivalent area rectangular cross sections at about every 1 km along the 34 km reach of the main channel in the Buffalo Cove region.

To facilitate model set up, the model coordinates were rotated 15.67° clockwise about the North. The coordinate rotation makes the vertical component of Y axis in the model system parallel to the main channel direction and the horizontal component of X axis to the floodplain flow condition. Figure 2 shows schematic local hydrodynamics in the study area. Flow pathways are well protected by high levees, thus water discharge per each cross section along the main river channel is conservative. The continuity constraint is given by:

$$Q_{C1}^{t} + Q_{F1}^{t} = Q_{C2}^{t} + Q_{F2}^{t} = Q_{C3}^{t} + Q_{F3}^{t} \tag{3}$$

where the superscript t represents time varying discharge (Q), subscript digits are cross section locations, and the subscript letters C and F represent the channel and floodplain, respectively. The channel flow from upstream to downstream results in more overbank flooding into the floodplain, thus the upstream channel discharge is greater than the downstream channel discharge (i.e. $Q_{C1}^{t} > Q_{C2}^{t} > Q_{C3}^{t}$). The upstream floodplain discharge is lower than the downstream floodplain discharge and floodplains around WMU1 and WMU2 are not flooded due to high levees which prevent overbank flow (i.e.$Q_{F3}^{t} > Q_{F2}^{t} > Q_{F1}^{t} = 0$).

Boundary conditions for fluvial flooding applications normally consist of the time-dependent discharge in the compound channel at the upstream end of the reach and the time varying water elevation or gradient at the downstream end of the channel [Bates *et al*., 2005]. Since there is no discharge station at the upstream boundary of the WMU1 domain, a virtual location C2 was created for which flow, Q_{C2}^{t} was estimated using an inverse distance squared weighting (IDW) interpolation with channel discharges Q_{C1}^{t} at Krotz Springs and Q_{C3}^{t} at Myette Point [Heijden and Haberlandt, 2010]. The upstream channel boundary condition is thus calculated as:

$$Q_{C2}^{t} = f(Q_{C1}^{t}, Q_{C3}^{t})_{IDW} = \frac{Q_{C1}^{t} \cdot d_{C2C3}^{2} + Q_{C3}^{t} \cdot d_{C1C2}^{2}}{d_{C1C2}^{2} + d_{C2C3}^{2}} \quad (4)$$

where d_{ij} is the distance between locations of i and j.

In addition to upstream channel discharge, upstream floodplain discharge is also set as a boundary condition. Although non-channel flow at the boundary of the domain is usually negligible for fluvial flooding applications [Bates *et al*., 2005], a time dependent floodplain discharge is necessary since the upper domain boundary crosses the floodplain and substantial flow crosses into the domain during the 62 day simulation period. The upstream floodplain discharge derived from Equation (3) and (4) (i.e. $Q_{F2}^{t} = Q_{C1}^{t} +$

$Q_{F1}^{t} - Q_{C2}^{t}$; $Q_{F1}^{t} = 0$) was distributed equally among all the upstream boundary grid cells.

For the downstream condition, water elevation data at Myette Point (H_{C3}^{t}) were used. The other boundaries of the domain within the rectangular grid are set to a free flux condition to force the model to calculate the slope used for the normal depth calculation between the last two points. Figure 3 shows daily time series of water elevations and discharges at gage stations. Gage stations are located at Krotz Springs (C1) and Myette Point (C3) along the main channel and at Buffalo Cove (B1) in the bayous, whereas C2 is a virtual station. The gage vertical datum are converted from the National Geodetic Vertical Datum of 1929 (NGVD29) into the National American Vertical Datum of 1988 (NAVD88) [Milbert, 1999] to fit the LiDAR floodplain elevations and bathymetry dataset from USACE. In this study, focus is on right (i.e. west) bank flooding in the Buffalo Cove WMU from the main channel of the Atchafalaya River.

To calibrate the model response to Manning's roughness coefficients, a matrix of 36 simulations was run with values of n_C varying from 0.020 to 0.030 in steps of 0.002 in the channel, and n_F varying from 0.05 to 0.30 in steps of 0.05 in floodplain. The range of values was chosen based on tables of typical n in various types of channels and floodplain [Chow, 1959]. Previous modeling in the Atchafalaya River Delta suggested that Manning's roughness coefficients in the area ranged from 0.01 to 0.06 for navigable waters, 0.01 to 0.02 for bayous, 0.03 to 0.06 for obstructed canals, and 0.2 to 0.5 for marsh and/or subaerial delta lobes [Donnel *et al*., 1991; Donnel and Letter, 1992].

The Mean Absolute Error (MAE) and bias were used to evaluate the sensitivity of the model to the range of Manning's coefficients, or:

$$MAE = \frac{1}{N}\sum_{i=1}^{N} |M_i - O_i| \quad (5)$$

$$bias = \frac{1}{N}\sum_{i=1}^{N} (M_i - O_i) \quad (6)$$

where M is model and O is observation (i.e. gage height or interferometry height differences). The MAE and bias were computed for all points where there were observations and were weighted equally. All model results for the total model period of 62 days are included in this calibration. Further details of both calibration approaches, using water elevations of gage measurements and water elevation changes from SAR interferometry, are described in 5.1 and 5.2, respectively.

4.2. SAR Interferometry

The Japan Aerospace Exploration Agency's (JAXA's) Advanced Land Observing Satellite (ALOS), a follow-on mission for the Japanese Earth Resources Satelite-1 (JERS-1), carries the Phased Array type L-band Synthetic Aperture Radar (PALSAR). The PALSAR scenes are HH polarized and L-band (wavelength: 23.62 cm). The incidence angles of PALSAR scenes are approximately 38.7° from descending passes. The PALSAR swath of path 168 and frame 590 were collected on 16 April 2008 and 1 June 2008. As illustrated in Figure 1, the SAR image covers the central Atchafalaya River Basin including the Buffalo Cove WMU.

Measurements of water elevation changes (dh/dt) for the model domain were obtained from repeat-pass PALSAR interferometry and are used in model calibration.

SAR Interferometric processing follows the two pass method [Massonnet e*t al.*, 1993]. The interferometric phase includes satellite orbit, topographic relief, and any changes in the radar range (i.e. floodplain water elevation change in this study). The orbit related phase is subtracted through flat earth phase removal that calculates satellite state vectors given by the system file and adjusts baseline errors based on the residual phase in the interferogram. As the most critical parameter in SAR interferometry, baseline is a measure of the distance between the two SAR antenna locations. The topographic related phase is subtracted using the Shuttle Radar Topography Mission (SRTM) C-band elevation data to make the remaining differential phase dependent on floodplain water elevation changes. Interferometrically measured water elevation changes in the direction of the radar line-of-sight (LOS) are converted to a vertical displacement in terms of the wavelength and incidence angle of the PALSAR scenes [Massonnet and Feigl, 1998]. In this processed interferogram, 2 π radians of interferometric phase are equivalent to 15.1 cm of vertical height change.

Figure 4 shows differential wrapped interferometric fringes in the floodplain. The patterns of a cycle of interferometric phase (i.e. fringe) imply that the basin consists of various independent hydrodynamic units as defined by the USACE (1982). Distinct changes in the interferometric dh/dt measurements are located along WMU boundaries. Most of the WMUs exhibit homogenous values in the interferogram. However, WMUs Buffalo Cove and Upper Bell River show sheet flow pattern and WMU Bayou DeGlais shows a sharp distinction in the middle of the floodplain due to a navigable waterway. The differential phase wrapped in a cycle of 2 π radians is unwrapped with minimum cost flow techniques and a triangular irregular network to provide water elevation changes. In the phase unwrapping stage, adaptive radar interferogram filtering is applied to reduce noise and enhance fringe visibility. The unwrapped differential phase corresponds to relative water elevation changes. The interferometric SAR measurements require a reference datum to convert from the relative water elevation changes to absolute values [Jung *et al.*, 2010]. For this reference datum, gage B1 was used, where the water level decreased 71 cm. (i.e. dh/dt = -71 cm over 46 days from 16 April 2008 to 1 June 2008, see h_{B1} in Figure 3b). The unwrapped and absolute interferometric measurements, shown in Figure 8c, were used to calibrate model water elevation changes.

5. Results

5.1. Calibration of Model Water Elevations (h) with Gage Measurement

LISFLOOD was first calibrated in terms of water elevations at the Buffalo Cove (B1) gage using a matrix of 36 simulations with various Manning's roughness coefficients of the channel (n_C and the floodplain, n_F. For each simulation, the MAE was computed based on the daily water elevation differences between model and gage measurement for the entire 62 day simulation period. The best-fit model of n_C and n_F was then determined as the lowest MAE in the three dimensional space plot of MAE, n_C and n_F. Figure 5 shows calibration surfaces for MAE and bias. The models with 0.022 to 0.026 in n_C and 0.10 to 0.20 in n_F show less than 10 cm in MAE. The optimum lies at 0.024 in n_C and 0.10 in n_F with 3.8 cm in MAE. The calibration surfaces show the L-shaped optimal region typical for 2D hydraulic models optimized against single gage or flood extent data (see for example Fewtrell *et al.*, 2011). Here an increase in channel friction can be compensated for by a decrease in floodplain friction (and vice versa) to yield identical MAE or global goodness of fit for a range of channel and floodplain friction combinations. It can be seen that as one moves away from the optimal L-shaped region, MAE is greater with increasing gradient.

The bias calibration surface shows that as n_C increases, bias increases and becomes less sensitive to n_F. It implies that modeling water elevations at gage B1 in bayous is more dependent on the Manning's roughness coefficient of the main channel relative to that of the surrounding floodplain. The generally positive bias means that modeled water elevations are greater than the gage measurement (see Equation 6). This agrees with the notion that water elevation and storage must increase since higher channel roughness decreases water velocity, thereby requiring a greater cross-section to maintain the same outflow. The daily time series of water elevation in the best-fit model is shown in Figure 6. It reveals that after 2 days of initiating the simulation, the model reaches a stable stage and the model results fit the gage water elevations within $\pm$ 4 cm MAE. This is an excellent result given typical terrain and discharge errors, and within an engineering study would likely be used to indicate a model that could be used to take flood risk management decisions. In scientific terms, it is however a relatively limited test since the model performance is only evaluated at a single point with the domain.

5.2. Calibration of Model Water Elevation Changes (dh/dt) with SAR Interferometry

The model is calibrated in terms of water elevation changes in the Buffalo Cove WMU using the same simulations as performed in 5.1. However, instead of using one *in* *situ* gage with a continuous height record, calibration is conducted using two images of height covering the entire flooded domain, separated by 46 days.

The MAE is again used to find the best-fit model of n_C and n_F against water elevation changes calculated from ALOS PALSAR interferometry from 16 April 2008 to 1 June 2008. Figure 7 shows calibration surfaces for MAE and bias. The models with 0.024 to 0.028 in n_C and 0.10 in n_F show a MAE of less than 8 cm over the 46 day period. The optimum lies at 0.028 in n_C and 0.10 in n_F with a MAE of 5.7 cm, which are similar but not identical to Manning's roughness coefficients calibrated in 5.1. The bias calibration surface shows that as n_F increases, bias decreases, being less sensitive to n_C. It implies that obtaining an optimal match between floodplain dh/dt measurements and the LISFLOOD-ACC model for the Buffalo Cove WMU is more dependent on the Manning's roughness coefficient of the floodplain compared to that of the main channel. The negative bias means that model water elevation change is actually less than that indicated by the interferometric measurements (see Equation 6). This is consistent with the notion that floodplain water elevations are less sensitive with higher roughness in the floodplain due to the lower floodplain velocities. Total frictional force (F) is proportional to Manning's roughness (n) and the square of flow velocity (v^2) so model sensitivity to friction is a non-linear function of the flow velocity (v). When v is low, the modeled water levels become dramatically less sensitive to n.

Figure 8 shows water elevation change maps calculated from the best-fit model and SAR interferometry. The modeled dh/dt is calculated by subtracting the water elevation map on 16 April 2008 from that on 1 June 2008. The interferometrically measured dh/dt in Figure 8 is absolute water elevation changes which are referenced and unwrapped from the differential wrapped interferogram in Figure 4. The dh/dt in Buffalo Cove WMU ranges from -100 to -50 cm over 46 days showing that the floodplain is draining over the this period. The largest difference in dh/dt between model and SAR interferometry is exhibited in the southwest part of the WMU. It appears that inside waterways hold floodwater moving from east to west and add more complexity into the local floodplain dynamics than is captured by this model. The Amazon floodplain channels are discovered to govern the complex water flow in the locally confined hydrodynamics [Alsdorf *et al*., 2007; Jung *et al*., 2010]. The interferometry demonstrates that the southwest part exhibits a distinct difference in the spatial gradients of water elevation changes as compared to the surrounding area, which is micro-terrain effects that are not predicted by the model in a 90 m grid,

5.3. Estimation of Water Storage Changes (dS/dt) in Buffalo Cove WMU

The daily modeled dS/dt is calculated by multiplying dh/dt by the grid cell area. The model dh/dt calibrated by SAR interferometry is used to calculate dS/dt.

$$dS^t/dt = S^t - S^{t-1} = \sum_{i=1}^{N}(h_i^t - h_i^{t-1}) \cdot dx \cdot dy \tag{7}$$

where t ranges from 1 to 62 as a simulation day and dx and dy are 90 m for a given grid box.

The time series dS/dt is shown in Figure 9a for daily as well as 5 and 10 day moving averages. The daily storage changes in the model domain of about 230 km^2 range approximately from $+10^7$ m^3/day to -10^7 m^3/day during the modeled period. The water storage changes are positive at the beginning whereas they turn to be negative after 27 April 2008 with some variations.

The relationship between the model water storage changes (dS/dt) and water elevation changes (dh/dt) at the Buffalo Cove gage (B1), shown in Figure 9b, shows a strong linear relationship, except for three outliers generated at the beginning of the simulation. It implies that the model requires more than 3 days to wet the whole floodplain and to provide reasonable values of water elevations in the floodplain of the WMU. The first polynomial regression model ($y = 2216650 \cdot x + 52421$; $y{:}\, dS/dt$, $x{:}\, dh/dt$) exhibits an R^2 of 0.94. The residuals of the regression model explain that $\mathrm{dh/dt}$ at the Buffalo Cove gage cannot be representative of dh/dt across all of the Buffalo Cove WMU floodplain. As can be seen in Figure 8, the dh/dt varies markedly in space. Maps of h and dh/dt in Figure 10 exhibit water storage changes that are positive, near zero, and negative. The maps of h show instances of floodplain filling and emptying. For instance, the average dh/dt of the WMU between 15 April 2008 and 16 April 2008 is 2.4 cm/day when the corresponding dS/dt is 5.5x10^6 m^3/day. On the contrary, the dh/dt average of the WMU between 31 May 2008 and 1 June 2008 is -2.9 cm/day when the corresponding dS/dt is -6.6x10^6 m^3/day. The dh/dt maps in the lower panel of Figure 10 show less variation within the WMU as compared to the dh/dt maps shown in Figure 8 because the time interval (dt) is 1 day shorter than 46 days in Figure 8.

6. Discussion

Two approaches to calibrate a 2D hydrodynamic model were investigated, one using a single *in situ* gage measurement and the second using SAR interferometry. Each approach calibrates the model in terms of different model products that have different space (i.e. dimensionality) and time scales. The first calibration uses time series of water elevations at one specified gage station for the total simulation period of 62 days. Due to the gage location in the bayou, the calibration shows more dependency on channel roughness relative to floodplain roughness.

The second calibration uses water elevation changes calculated from SAR interferometry across the whole WMU area for one time interval of 46 days between two successive overpasses of the PALSAR satellite. The latter is a particularly stern test for a 2D hydrodynamic model as to require accurate prediction of spatial patterns of water elevation change over a long simulation period. Since SAR interferometry receives strong scatters in the floodplain due to the double bounce effect as compared to specular scattering of open water [Lu and Kwoun, 2008; Jung and Alsdorf, 2010], this calibration shows more dependency on floodplain roughness.

Most 2D floodplain modeling requires a longer spin-up time, as compared to 1D channel modeling, in order to wet the floodplain as well as channel for stabilization of the floodplain dynamic in the model. The spin-up time in the calibration with SAR interferometry requires at least 3 days more than the 2 days required with only gage measurements. The different calibration methods suggest the same floodplain roughness, but different channel roughness in their best-fit models, which can be explained by different model products used in their calibrations. The pattern and trend of the MAE and bias calibration surfaces imply that calibration against different data sets would lead a user to make different conclusions regarding the model's differential sensitivity to channel and floodplain friction. Practically, the real meaning of roughness as an effective parameter is a component of topography that has to be calculated to optimize the agreement between model predictions and measurements [Lane, 2005]. The calibrated roughness can be a valuable reference to the hydrodynamic modeling community as it is properly adjusted along water stage, grid resolution, and model feature.

The impact of the results to uncertainty in upstream discharge was investigated by changing the flow by +/- 20 percent in increments of 5 %, for both calibration approaches. Root-Mean-Square-Deviation (RMSD) in the modeled h and dh/dt was computed for each flow, averaged across the domain, using the best-fit model of 0.028 in n_C and 0.10 in n_F. Assuming that even for good gages, Q error is likely to be ± 10 %., Figure 11 indicates that this likely error in upstream Q leads ~10 cm of errors in the modeled h maps on both 16 April 2008 and 1 June 2008 and less than 2.5 cm in the modeled dh/dt map (Figure 11). This implies that the effect of an error in Q on the absolute water elevations is much larger than the effect of the same Q error on the water elevation changes. The deviation on absolute water elevations can be compensated for in any modeling study with a uniform offset derived from a contemporaneous ground truth campaign. The deviation of 2.5 cm in the modeled dh/dt can be regarded as the range of acceptable differences between the observed dh/dt and the modeled one. It suggests that within the Q ± 10 % error ranges, 54 % of dh/dt map in Figure 8d shows a good agreement between the model and the interferometric measurement. The slight difference in channel roughness between two calibration methods (i.e. 0.024 / 0.1 and 0.028 / 0.1 in n_C / n_F, respectively) leads ~1.5 cm of the modeled dh/dt difference in Figure 7a and this can be also explained by within the Q ± 10 % error ranges.

SAR interferometry with a short baseline is the more appropriate to provide water elevation changes and calibrate the corresponding model products as compared to long baseline. Short perpendicular components in the baseline yield more topographic relief per phase cycle than long baselines, thus more reliable estimates of water elevation changes [Zebker and Villasenor, 1992]. In this study, the ALOS PALSAR L-band interferogram were processed with a perpendicular baseline of -219 m at the center of the satellite acquisition. The short baseline indicates that 2 π radians of phase are equivalent to ~204 m of topographic relief (i.e. the ambiguity height) whereas depending on the incidence angle, the same 2 π radians are also equivalent to about 15.1 cm of vertical water elevation change [Massonnet and Feigl, 1998]. The short perpendicular baselines and the C-band SRTM relative height errors of 5.5 m [Farr *et al*., 2007] cause 0.17 radians of phase change, which are equivalent to 0.4 cm of vertical displacement. The accuracy of this displacement measurement is a function of the local coherence as well as of our ability to separate the topographic phase component from the total observed phase. The mean coherence of 0.35 in the modeled floodplain yields an expected phase noise value of less than 0.4 radian error for 21 looks used in the processing [Zebker and Villasenor, 1992; Li and Goldstein, 1990], which is equivalent to less than 1.0 cm of vertical displacement. The scale errors in the observed dh/dt are small enough to calibrate the modeled dh/dt and provide the optimum Manning's roughness.

In both gage stage h and interferometric SAR dh/dt calibrations, the tolerable difference between model and data is much smaller as some of key errors drop out. Error sources in the LiDAR data, a terrain data error resulting from the averaging to 90 m, the observed h data, and the measured dh/dt are less than 1 cm whereas the likely ±10%

errors in Q result in less than 2.5 cm in the modeled dh/dt. It is noted that these errors are not necessarily additive and not all will be at a maximum at the same time.

This model domain is mostly covered with woody wetland, yet the Atchafalaya River Basin includes more various land covers of urban, pasture, cultivated crops, woody wetlands, and emergent herbaceous wetlands in 2006 National Land Cover Data (NLCD) distributed by USGS [Fry *et al*, 2011]. For large floodplain modeling, the roughness can be assigned in more detail based on land use and land cover [Kalyanapu *et al*., 2009]. To take advantage of land cover data to the roughness assignment, optimization algorithms need to be utilized for multi parameter calibration [Zhang *et al*., 2008].

7. Conclusions

The 2D LISFLOOD-ACC model was applied to spring flooding in the central Atchafalaya River Basin and calibrated using two independent approaches. A traditional approach used a continuous temporal record of *in situ*, point water level gage measurements. The second new approach, employed temporal (dh/dt) and spatial (dh/dx, dh/dy) variations of water levels derived from ALOS PALSAR interferometry, observed at two separate times. Although the two different approaches yielded slightly different values for channel Manning's n, the close comparison in results establish the feasibility of satellite based approach, at least for this particular basin and flow conditions. Results were facilitated by a relatively simple spring hydrograph with few spikes in river discharge, and well defined floodplain boundaries. Overall, the results offer a new approach for satellite-based calibration of hydrodynamic models, especially in regions of sparse *in situ* data.

The slight difference in calibration results are to be expected given that the two independent approaches relied on two different data sets, in one case a continuous time series of channel elevations at a single point, and in the second, a continuous spatial distribution of water levels and slopes at two points in time. However, differences also might be due to artifacts in the observed data, or micro-terrain effects that are not picked up in a 90 m grid, or error associated with assumptions in the hydraulic model. Results indicate that even a few observations can quantify the floodplain water elevation and reveal the complexity of the floodplain hydrodynamics. This study highlights the importance and potential advantage of 2D interferometric SAR techniques to support 2D floodplain model calibration.

Second, results on the spatial and temporal variations of water elevations ($\frac{dh/dt}{dx}$, $\frac{dh/dt}{dy}$) are demonstrated to be useful to estimate daily time series of water storage changes (dS/dt) in Buffalo Cove WMU. Since the model is validated in terms of dh/dt from SAR interferometry, the improved model can generate reliable estimates of dS/dt and the moving averages can be useful to see the trend of basinwide water storage changes.

Lastly, results indicate the feasibility of using SAR interferometry for enhanced prediction and assessment capabilities for future flood events in the floodplain. The hydrodynamic modeling calibrated by SAR interferometry can be extended into higher grid resolution and/or larger domains to study the floodplain hydrodynamics in more detail. For the purpose of future flood control and risk management, modeling could focus on monitoring the basin in near real time with the help of parallel computation using multi core processors.

Acknowledgement

This research was supported by an appointment to the NASA Postdoctoral Program (NPP) at the Goddard Space Flight Center (GSFC), administered by Oak Ridge Associated Universities (ORAU) through a contract with NASA. We acknowledge the NASA Center for Climate Simulation (NCCS) and the Ohio Supercomputer Center (OSC) for use of the computing resources. The Ohio State University (OSU) component of the research is partially supported by NASA's Hydrology Program and OSU's Climate, Water and Carbon Program. We thank Yvonne Allen in USACE for sharing her knowledge of the Atchafalaya River Basin. LiDAR data were undertaken and provided by USGS National Geospatial Program and USGS Coastal and Marine Geology Program. ALOS PALSAR data were provided by Alaska Satellite Facility (ASF).

References

Allen, Y. C., G. C. Constant, and B. R. Couvillion (2008), Preliminary classification of water areas within the Atchafalaya Basin floodway system by using Landsat imagery, U.S. Geological Survey, Open-File Report 2008-1320.

Alsdorf, D., P. Bates, J. Melack, M. Wilson, and T. Dunne (2007), Spatial and temporal complexity of the Amazon flood measured from space, *Geophys. Res. Lett.*, 34, L08402, doi:10.1029/2007GL029447.

Alsdorf, D. E., T. Dunne, J. M. Melack, L. C. Smith, and L. L. Hess (2005), Diffusion modeling of recessional flow on central Amazonian floodplains, *Geophys. Res. Lett.,* 32, L21405, doi:10.1029/2005GL024412.

Alsdorf, D. E. (2003), Water storage of the central Amazon floodplain measured with GIS and remote sensing imagery, *Ann. Assoc. Amer. Geographers*, 93, 55-66.

Alsdorf, D. E., J. M. Melack, T. Dunne, L. A. K. Mertes, L. L. Hess, and L. C. Smith (2000), Interferometric radar measurements of water level changes on the Amazon floodplain, *Nature*, 404, 174-177.

Bates, P. D., M. S. Horritt, and T. J. Fewtrell (2010), A simple inertial formulation of the shallow water equations for efficient two-dimensional flood inundation modelling, *J. Hydrol.,* 387, 33-45.

Bates, P. D., R. J. Dawson, J. W. Hall, M. S. Horritt, R. J. Nicholls, J. Wicks, and M. A. A. M. Hassan (2005), Simplified two-dimensional numerical modelling of coastal flooding and example applications, *Coast. Eng.,* 52, 793-810.

Bates, P. D., and A. P. J. De Roo (2000), A simple raster-based model for floodplain inundation, *J. Hydrol.*, 236, 54-77.

Bates, P. D., M. G. Anderson, L. Baird, D. E. Walling, and D. Simm (1992), Modelling floodplain flow with a two-dimensional finite element scheme, *Earth Surf. Process. Landf.*, 17, 575-588.

Bradbrook, K. F., S. N., Lane, S. G. Waller, and P. D. Bates (2004), Two-dimensional diffusion wave modelling of flood inundation using a simplified channel representation, *Int. J. River Basin Manage.,* 3, 211-223.

Chow, V. T. (1959), Open channel hydraulics, McGraw-Hill, New York.

DHI Water and Environment (2001), MIKE11 hydrodynamic reference manual, DHI, Horshølm, Denmark

Di Baldassaarre, G., G. Schumann, and P. D. Bates (2009), A technique for the calibration of hydraulic models using uncertain satellite observations of flood extent, *J. Hydrol.*, 367, 276-282.

Donnell, B. P., and J. V. Letter (1992), The Atchafalaya River Delta Report 12: two-dimensional modeling of alternative plans and impacts on the Atchafalaya bay and Terrebonne marshes, U.S. Army Engineer District, New Orleans, Louisiana, AD-A246 089.

Donnell, B. P., J. V. Letter, and A. M. Tetter (1991), The Atchafalaya River Delta Report 11: two-dimensional modeling, U.S. Army Engineer District, New Orleans, Louisiana, AD-A237 639.

Ervine, D. A. and A. B. MacCleod (1999), Modelling a river channel with distant floodbanks, *Proc. Inst. Civil. Eng.-Wat. Marit. Energy*, 136, 21-33.

Falconer, R. A. (1986), A water quality simulation study of a natural harbor, American Society of Civil Engineers, *J. Waterw. Port Coast. Ocean Eng.-Asce.*, 112, 1, 15-34.

Farr, T., and 17 others (2007), The Shuttle Radar Topography Mission, *Rev. Geophys.*, 45, RG2004, doi:10.1029/2005RG000183.

Fewtrell, T. J., J. C. Neal, P. D. Bates, and P. J. Harrison (2011), Geometric and structural model complexity and the prediction of urban inundation. *Hydrol. Processes*, 25, 3173-3186.

Fread. D. L. (1984), Flood routing, In: M. G. Anderson and t. P. Burt (eds), Hydrological Forecasting, Hohn Wiley and Sons, Chichester, Chapter 14.

Fry, J., G. Xian, S. Jin, J. Dewitz, C. Homer, L. Yang, C. Barnes, N. Herold, and J. Wickham (2011), Completion of the 2006 National Land Cover Database for the Conterminous United States, *Photogramm. Eng. Remote Sens.,* 77, 858-864.

Heijden, S., and U. Haberlandt (2010), Influence of spatial interpolation methods for climate variables on the simulation of discharge and nitrate fate with SWAT, *Adv. Geosci.*, 27, 91-98.

Halcrow and HR Wallingford (2001), ISIS flow user manual, vol. 1 user guide, HR Wallingford.

Hess, L. L., J. M. Melack, S. Filoso, and Y. Wang (1995), Delineation of inundated area and vegetation along the Amazon floodplain with the SIR-C synthetic aperture radar, *IEEE Trans. Geosci. Remote Sensing*, 33, 896-904.

Horritt, M. S. and P. D. Bates (2001). Effects of spatial resolution on a raster based model of flood flow, *J. Hydro.*, 253, 239-249.

Hunter, N. M., P. D. Bates, S. Neelz, G. Pender, I. Villanueva, N. G. Wright, D. Liang, R. A. Falconer, B. Lin, S. Waller, A. J. Crossley, and D. Mason (2008), Benchmarking 2D hydraulic models for urban flooding, *Proc. Inst. Civil. Eng.-Water Manag.,* 16, 13–30.

Jung, H. C., J. Hamski, M. Durand, D. Alsdorf, F. Hossain, H. Lee, A. K. M. A. Hossain, K. Hasan, A. S. Khan, and A. K. M. Z. Hoque (2010), Characterization of complex fluvial systems via remote sensing of spatial and temporal water level variations, *Earth Surf. Processes Landforms*, 35, 294-304.

Jung, H. C., and D. Alsdorf (2010), Repeat-pass multi-temporal interferometric SAR coherence variations with Amazon floodplain and lake habitats, *Int. J. Remote Sens.*, 31, 881-901.

Kalyanapu, A., S. J. Burian, and T. N. McPherson (2009), Effect of land use-based surface roughness on hydrologic model output, *J. Spat. Hydrol*., 9, 51-71.

Kim, J., Z. Lu, H. Lee, C. K. Shum, C. M. Swarzenski, T. W. Doyle, and S. Baek (2009), Integrated analysis of PALSAR/Radarsat-1 InSAR and ENVISAT altimeter data for mapping of absolute water level changes in Louisiana wetlands, *Remote Sens. Environ.,* 113, 2356-2365.

Knabb, R. D., D. P. Brown, and J. R. Rhome (2007), Hurricane Rita, National Hurricane Center.

Knabb, R. D., J. R. Rhome, and D. P. Brown (2006), Tropical cyclone report: Hurricane Katrina: 23-30 August 2005, National Hurricane Center.

Lake Pontchartrain Basin Foundation (LPBF) (2010), Hydrology and hydrodynamic modeling of the Mississippi River in southeast Louisiana, report, part I, Lake Pontchartrain Basin Foundation, Metairie, LA.

Lake Pontchartrain Basin Foundation (LPBF) (2008), Comprehensive recommendations supporting the use of the multiple lines of defense strategy to sustain coastal Louisiana, report, version 1, Lake Pontchartrain Basin Foundation. Metairie, LA.

Lane, S. N. (2005), Roughness – time for a re-evaluation?, *Earth Surf. Processes Landforms,* 30, 251-253.

Li, F. K., and R. M. Goldstein (1990), Studies of multibaseline spaceborne interferometric synthetic aperture radars, *IEEE Trans. Geosci. Remote Sensing*, 28, 88-97.

Lee, H., C. K. Shum, Y. Yi, M. Ibaraki, J. Kim, A. Braun, C. Kuo, and Z. Lu (2009), Louisiana wetland water level monitoring using retracked TOPEX/POSEIDON altimetry, *Mar. Geod.,* 32, 284-302.

Louisiana Department of Natural Resources (LDNR) (2010), Atchafalaya Basin: FY 2010 annual plan, Atchafalaya Basin Program.

Lu, Z., J. Kim, H. Lee, C. Shum, J. Duan, M. Ibaraki, O. Akyilmaz, and C. Read, (2009), Helmand River hydrologic studies using ALOS PALSAR InSAR and ENVISAT altimetry, *Mar. Geod.,* 32, 320-333.

Lu, Z. and O. Kwoun (2008), Radarsat-1 and ERS InSAR analysis over southeastern coastal Louisiana: implications for mapping water-level changes beneath swamp forests, *IEEE Trans. Geosci. Remote Sens.*, 46, 2167-2184.

Lu, Z., M. Crane, O. Kwoun, C. Wells, C. Swarzenski, and R. Rykhus (2005), C-band radar observes water level change in swamp forests. *EOS*, 86, 141-144.

Massonnet, D., and K. L. Feigl (1998), Radar interferometry and its application to changes in the Earth's surface, *Rev. Geophys.*, 36, 441–500.

Massonnet, D., M. Rossi, C. Carmona, F. Adragna, G. Peltzer, K. Feigl, and T. Rabaute (1993), The displacement field of the Landers earthquake mapped by radar interferometry, *Nature,* 364, 138–142.

Meade, R. H. (1995), Contaminants in the Mississippi River 1987-92, U.S. Geological Survey Circular, 1133.

Milbert, D. G. (1999), National Geodetic Survey (NGS) height conversion methodology, VERTCON, NGS.

Neal, J. G. Schumann, T. Fewtrell, M. Budimir, P. Bates, and D. Mason (2011), Evaluating a new LISFLOOD-FP formulation with data from the summer 2007 floods in Twekesbury, UK, *J. Flood Risk Manag.*, 4, 88-95.

Neal, J. C., T. J. Fewtrell, and M. A. Trigg (2009), Parallelisation of storage cell flood models using OpenMP, *Environ. Modell. Software*, 24, 872–877.

Rodriguez, E., C. S. Morris, and J. E. Belz (2006), A global assessment of the SRTM performance, *Photogramm. Eng. Remote Sens*., 72, 249–260.

Samuels, P. G. (1990), Cross section location in one-dimensional model, In W. R. White (ed), International Conference on River Flood Hydraulics, John Wiley and Sons, Chichester, 339-350.

Samuels, P G., and M. P. Gray (1982), The FLUCOMP river model package – an engineers guide, Report No. EX 999, HR Wallingford.

Smith, L. C. (1997), Satellite remote sensing of river inundation area, stage, and discharge: a review, *Hydrol. Processes,* 11, 1427-1439.

Syme, W. J. (1991), Dynamically linked two-dimensional/one-dimensional hydrodynamic modelling program for rivers, estuaries and coastal water, MEngSc Thesis, University of Queensland, Australia.

Templet, P., and K. Meyer-Arendt (1988), Louisiana wetland loss: a regional water management approach to the problem, *Environ. Manage,* 12, 181–192.

U.S. Army Corps of Engineers (USACE) (2011), Morganza floodway, http://www.mvn.usace.army.mil/bcarre/morganza.asp, retrieved on 24 October 2011.

U.S. Army Corps of Engineers (USACE) (2006), Atchafalaya River system hydrographic survey book, New Orleans District, LA.

U.S. Army Corps of Engineers (USACE) (2001), HEC-RAS river analysis system, hydraulic reference manual, version 3.0, Hydrologic Engineering Center, Davis, CA.

U.S. Army Corps of Engineers (USACE) (1982), Atchafalaya Basin floodway system feasibility study, main report and final environmental impact statement, New Orleans District, LA.

U.S. Environmental Protection Agency (USEPA) (1987), Saving Louisiana's coastal wetlands: the need for a long-term plan of action, report of the Louisianan wetland protection panel, EPA-230-02-87-026.

U.S. Geological Survey (USGS) (2011), 2010 Lidar elevation map for the Atchafalaya basin, http://abp.cr.usgs.gov/Library/Default.aspx?keyword=Lidar, retrieved on 24 August 2011.

Vaughn, D. M., D. Rickman, and H. Oscar (1996), Modeling spatial and volumetric changes in the Atchafalaya Delta, Louisiana, *Geocarto Int*., 11, 71-80.

Villanueva, I. and N. G. Wright (2006), Linking Riemann and storage cell models for flood prediction, *Proc. Inst. Civil. Eng.-Water Manag*., 159, 1, 27-33.

Walker, J., J. Coleman, H. Roberts, and R. Tye (1987), Wetland loss in Louisiana, *Geogr. Ann.,* 69, 189–200.

Wang, F. C., V. Ransibrahmanakul, K. L. Tuen, M. L. Wang, and F. Zhang (1995), Hydrodynamics of a tidal inlet in Fourleague Bay/Atchafalaya Bay, Louisiana, *J. Coastal Res.*, 11, 733-743.

Wilson, M., P. Bates, D. Alsdorf, B. Forsberg, M. Horritt, J. Melack, F. Frappart, and J. Famiglietti (2007), Modeling large-scale inundation of Amazonian seasonally flooded wetlands, *Geophys. Res. Lett.*, 34, L15404, doi:10.1029/2007GL030156.

Yu, D., and S. N. Lane (2011), Interactions between subgrid-scale resolution, feature representation and grid-scale resolution in flood inundation modelling, *Hydrol. Processes,* 25, 36-53.

Zanobetti, D., H. Longeré, A. Preissmann, and J. A. Cunge (1970), Mekong delta mathematical model program construction, *Proc. Amer. Soc. Civil Eng., J. Waterw. Harbors Div.*, 96, 181–199.

Zebker, H. A., and J. Villasenor (1992), Decorrelation in interferometric radar echoes, *IEEE Trans. Geosci. Remote Sens.,* 30, 950-959.

Zhang, X., R. Srinivasan, K. Zhao, and M. V. Liew (2008), Evaluation of global optimization algorithms for parameter calibration of a computationally intensive hydrologic model, *Hydrol. Processes,* 23, 430-441.

Figure Captions

Figure 1. LiDAR map over the study area. The Atchafalaya River Basin is bounded on the east and west sides by levees in south central Louisiana, United States. The upstream main channel in the basin diverts the Lower Mississippi River and flows out to the Gulf of Mexico. The orange rectangular box locates hydrodynamic model study area and green diagonal box indicates the ALOS PALSAR swath used in this study. The Atchafalaya River and Mississippi River are represented by blue lines. Levees and gages are marked with red lines and inverted black triangles. Gage stations are located at Krotz Springs (C1) and Myette Point (C3) along the main channel and at Buffalo Cove (B1) in bayou whereas C2 is a virtual station.

Figure 2. Schematic of local hydrodynamics in the Atchafalaya River Basin including 13 water management units (WMUs): 1-Lake Henderson , 2-Alabama Bayou, 3-Werner, 4-Lost Lake, 5-Cow Island, 6-Bayou DeGlais, 7-Cocodrie Swamp, 8-Pigeon Bay, 9-Beau Bayou, 10-Flat Lake, 11-Buffalo Cove, 12-Upper Bell River, 13-Six Mile Lake [USACE, 1982]. Black and light blue arrows are indicative of channel and floodplain flow directions. Light blue dotted lines represent floodplain flow boundary condition segments in the model. These lines are normal to the main channel direction between C2 and C3.

Figure 3. Daily time series of water discharges and elevations at gages in the model area during 2008. Panels (a) and (b) show a one year hydrograph including the model period during high water. The solid lines represent the first and last day in simulation on 1 April 2008 and 1 June 1 2008. Channel water elevations H_{C3} and H_{B1} are required for

downstream channel boundary condition and calibration, respectively. Channel discharge Q_{C2} and floodplain discharge Q_{F2} are collected and calculated for upstream boundary condition. Panels (c) and (d) are fitted in the model period. The vertical dashed lines represent the ALOS PALSAR acquisition dates on 16 April 2008 and 1 June 2008.

Figure 4. Differential wrapped interferogram of L-band PALSAR superimposed on the image reflectivity map in the Atchafalaya River Basin. The orange rectangular box locates the LISFLOOD model area. The color scale represents one cycle of interferometric phase that can be interpreted as 15.1 cm in vertical displacement. These fringes represent water elevation changes between 16 April 2008 and 1 June 2008.

Figure 5. Calibration surfaces for mean absolute error (left) and bias (right) in terms of water elevations at gage Buffalo Cove (B1) as function of channel (horizontal axis) and floodplain (vertical axis) Manning's roughness coefficients. The optimum roughnesses, determined as the lowest MAE equal to 3.8 cm, lies at 0.024 for channel n_c and 0. 10 for floodplain n_f.

Figure 6. Model water elevations compared to actual water elevations at gage Buffalo Cove (B1). The model after 2 days in simulation starts to fit the gage water elevations within $\pm$ 4 cm in MAE with Manning's roughness coefficients of 0.024 in the channel and 0.10 in the floodplain.

Figure 7. Calibration surfaces for mean absolute error (left) and bias (right) in terms of water elevation changes in the Buffalo Cove WMU as function of channel (horizontal axis) and floodplain (vertical axis) Manning's roughness coefficients (n). The optimum lies at 0.028 for channel $n_c$and 0. 10 for floodplain n_f with 5.7 cm MAE for the 46 day simulation.

Figure 8. (a) Water elevation maps on April 16 2008 (upper) and June 1 2008 (lower). (b) Water elevation change map calculated from the calibrated model. (c) Water elevation change map from SAR interferometry. (d) Difference of water elevation change from between the model (b) and the SAR interferometry (c).

Figure 9. (a) Daily time series of water storage changes in the area of ~230 km^2 in the Buffalo Cove WMU. The 5 and 10 day moving averages are performed to demonstrate the trend of the water storage changes. (b) Relationship between model dS/dt in Buffalo Cove WMU and dh/dt at the Buffalo Cove gage (B1). The goodness of fit (R^2) is 0.94 based on the first polynomial regression model without three outliers that are generated before the model is stabilized.

Figure 10. (Upper) Water depth maps relative to the LiDAR floodplain elevation, and (lower) water depth change maps when dS/dt is positive (a), near zero (b), and negative (c).

Figure 11. Results of the modeled h and dh/dt to uncertainty in upstream Qs, varying from -20 % and 20 % in steps of 5 %. The calibrated model of 0.028 in n_C and 0.10 in n_F is used as a behavioral model. The h maps on 16 April 2008 and 1 June 2008 and dh/dt map for the 46 days are shown in Figure 8a and 8b.

Figures

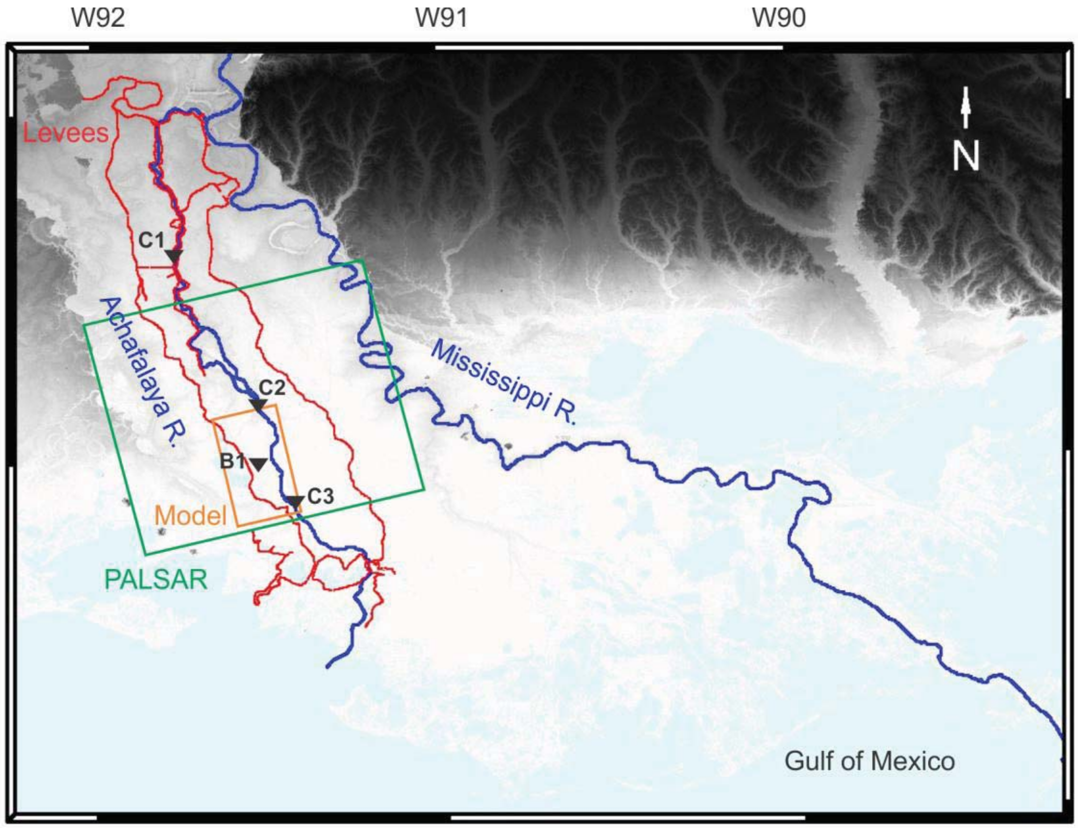

Figure 1.

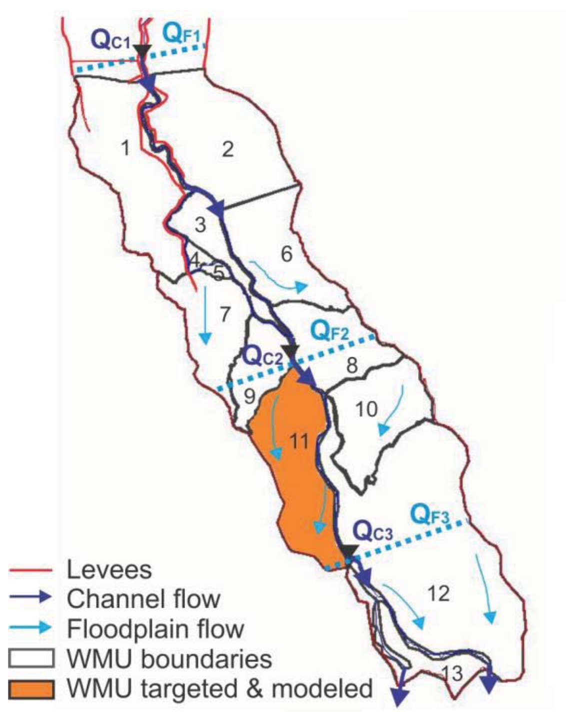

Figure 2.

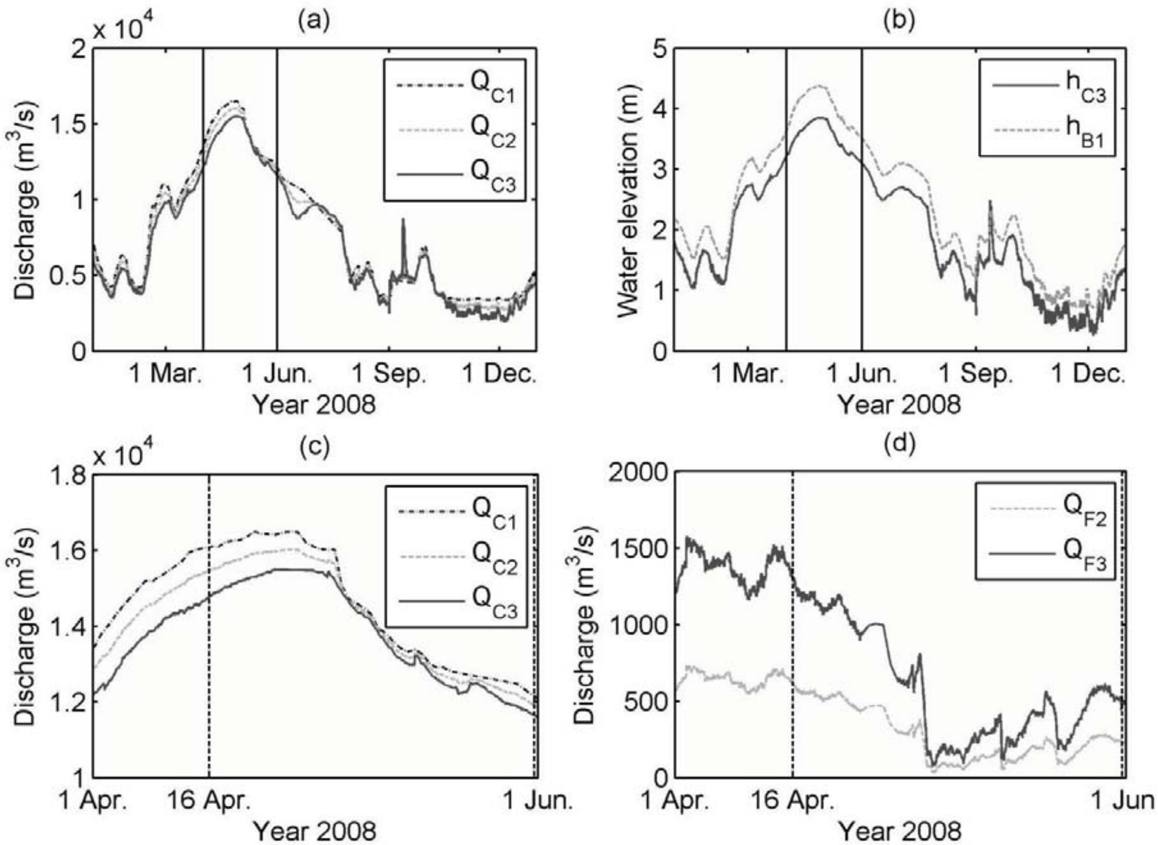

Figure 3.

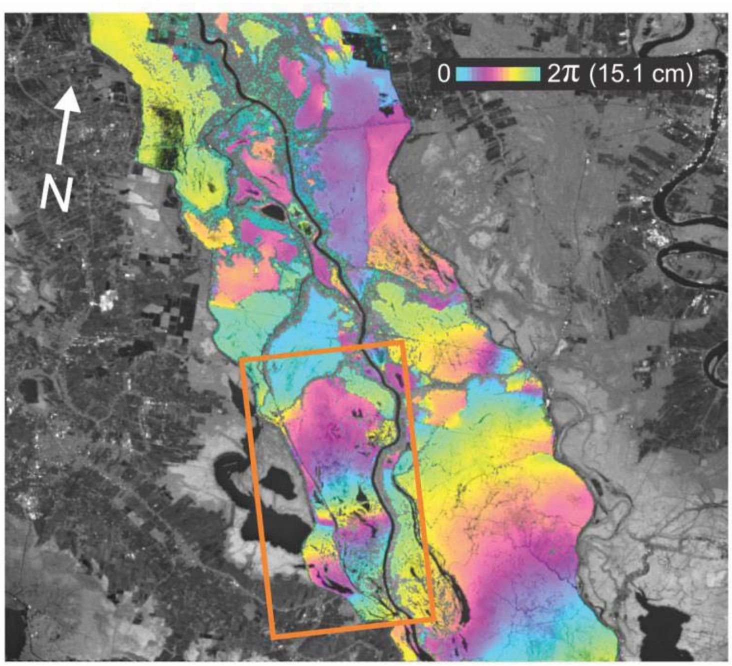

Figure 4.

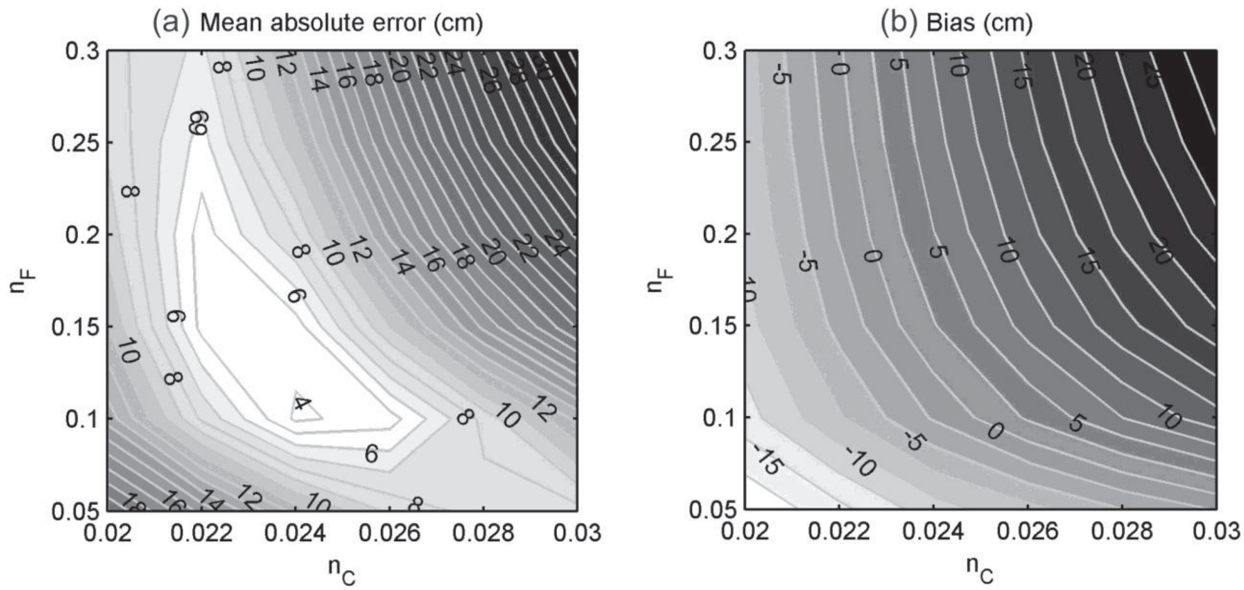

Figure 5.

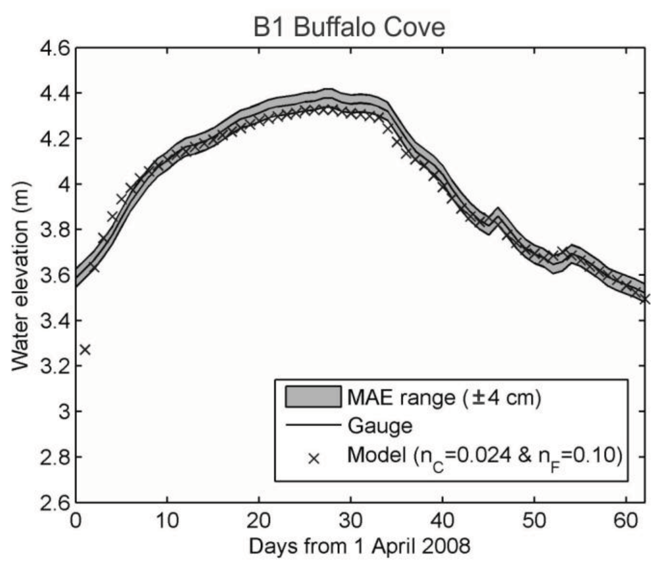

Figure 6.

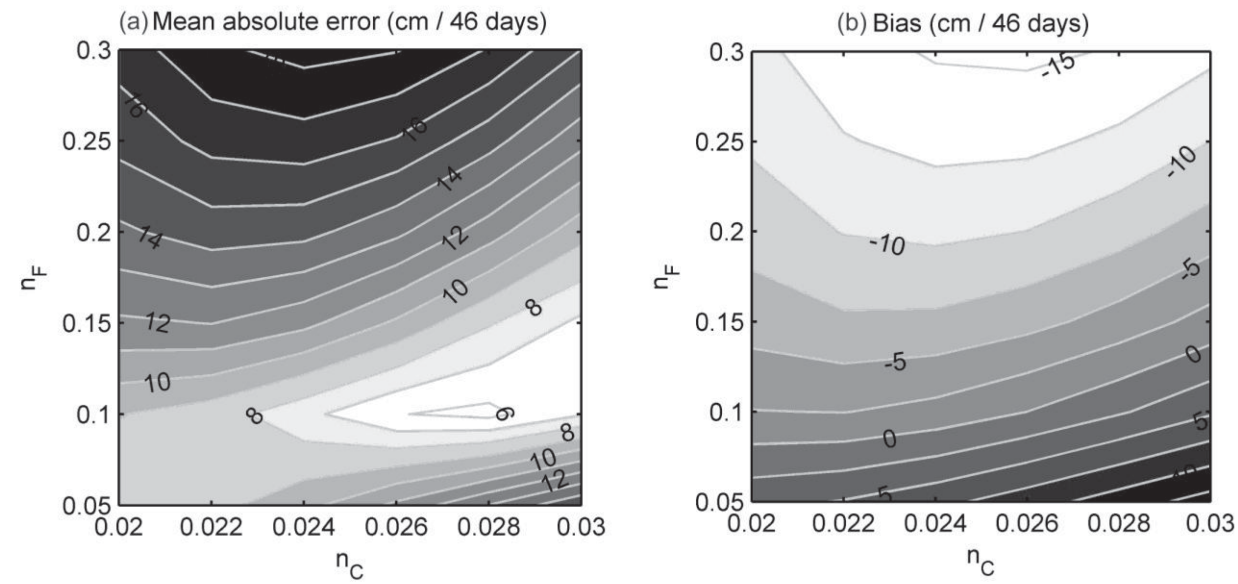

Figure 7.

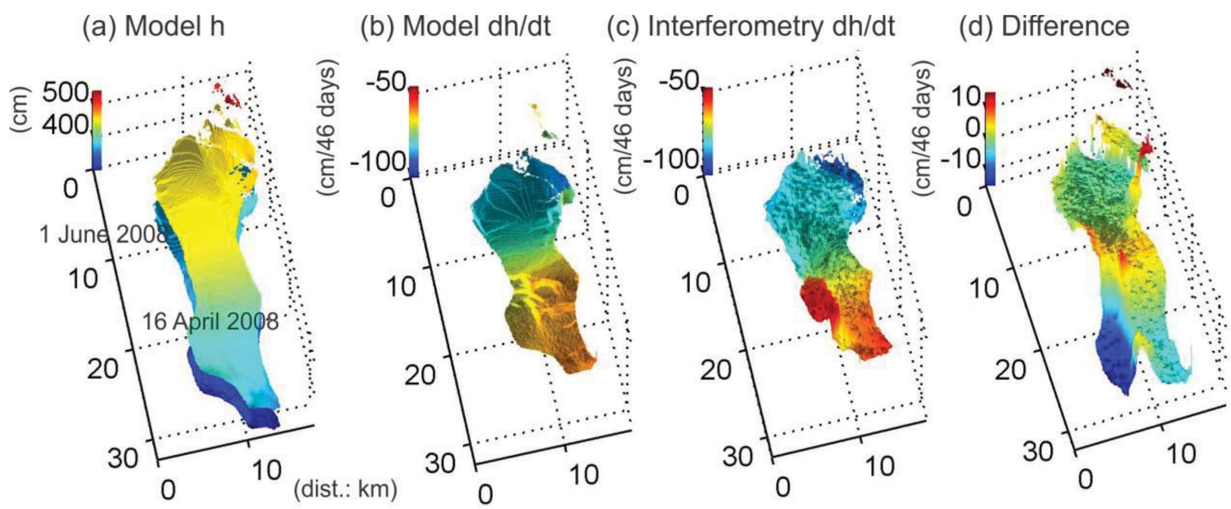

Figure 8.

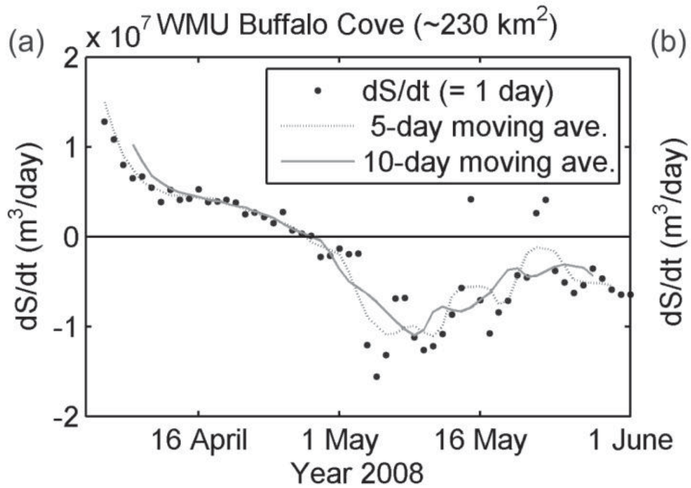

Figure 9.

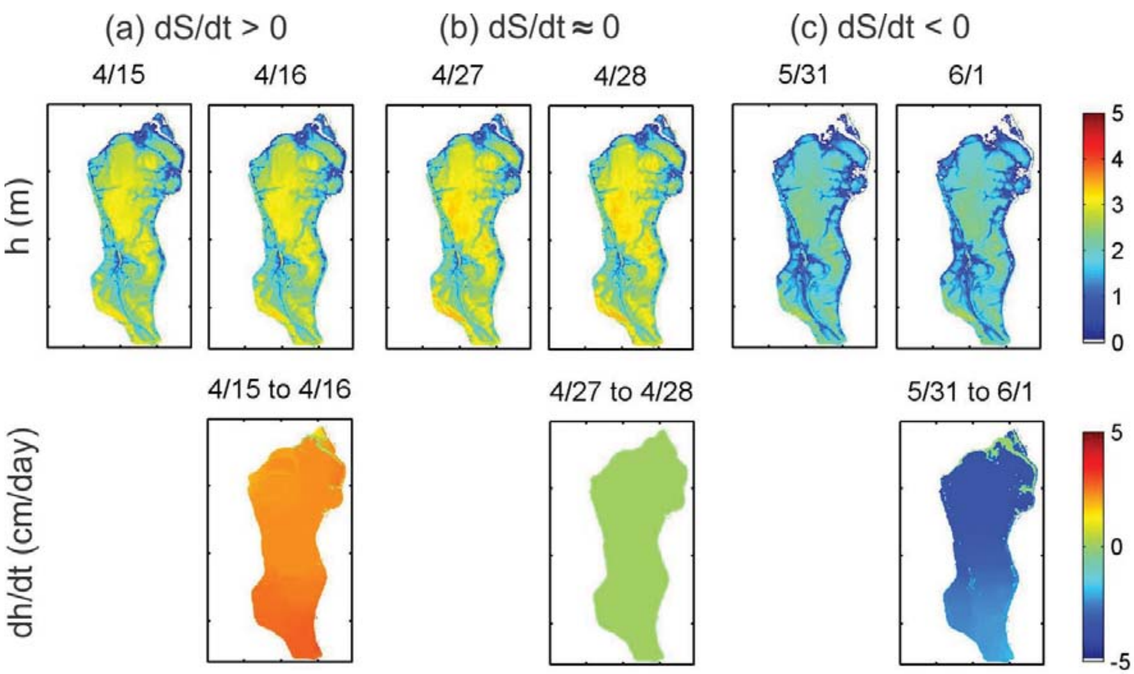

Figure 10.

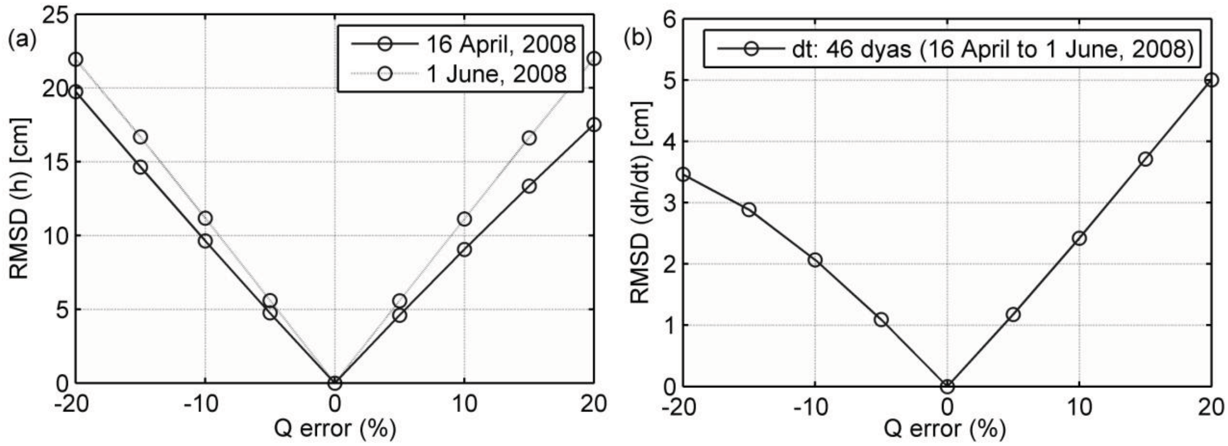

(a)
16 April, 2008
1 June, 2008
RMSD (h) [cm]
Q error (%)
(b)
dt: 46 dyas (16 April to 1 June, 2008)
RMSD (dh/dt) [cm]
Q error (%)

Figure 11.